# Molecular binding of $Eu^{III}/Cm^{III}$ by *Stenotrophomonas bentonitica* and its impact on the safety of future geodisposal of radioactive waste

Miguel A. Ruiz-Fresneda[1,*], Margarita Lopez-Fernandez[1,*,#], Marcos F. Martínez-Moreno[1], Andrea Cherkouk[2], Yon Ju-Nam[3], Jesús J. Ojeda[3], Henry Moll[2], Mohamed L. Merroun[1]

[1]Department of Microbiology, University of Granada, Granada, Spain

[2]Institute of Resource Ecology, Helmholtz-Zentrum Dresden-Rossendorf e.V., Dresden, Germany

[3]Systems and Process Engineering Centre, College of Engineering, Swansea University, Swansea, UK

[*]Corresponding author/s: Miguel Angel Ruiz-Fresneda. Email: mafres@ugr.es; Margarita Lopez-Fernandez. Email: margaritalopez@ugr.es

[#]Present address: Institute of Resource Ecology, Helmholtz-Zentrum Dresden-Rossendorf e.V., Dresden, Germany

## 1. Abstract

Microbial communities occurring in reference materials for artificial barriers (*e.g.* bentonites) in future deep geological repositories of radioactive waste can influence the migration behavior of radionuclides such as curium ($Cm^{III}$). This study investigates the molecular interactions between $Cm^{III}$ and its inactive analogue europium ($Eu^{III}$) with the indigenous bentonite bacterium *Stenotrophomonas bentonitica* at environmentally relevant concentrations. Potentiometric studies showed a remarkable high concentration of phosphates at the bacterial cell wall compared to other bacteria, revealing the great potential of *S. bentonitica* for metal binding. Infrared spectroscopy (ATR-FTIR) and X-ray photoelectron spectroscopy (XPS) confirmed the role of phosphates and carboxylate groups from the cell envelope in the bioassociation of $Eu^{III}$. Additionally, time-resolved laser-induced fluorescence spectroscopy (TRLFS) identified phosphoryl and carboxyl groups from bacterial envelopes, among other released complexing agents, to be involved in the $Eu^{III}$ and $Cm^{III}$ coordination. The ability of this bacterium to form a biofilm at the surface of bentonites allow them to immobilize trivalent lanthanide and actinides in the environment.

**Keywords**: europium, curium, bacterial speciation, mobility, geodisposal

## 2. Introduction

The safe disposal of radioactive waste is crucial to ensure the safety of future generations, as well as for the biosphere. The implementation of deep geological repositories (DGRs) is planned in the near future for the disposal of high level (HLW) and long-lived radioactive wastes, which are the most hazardous since they contain larger radionuclide concentrations and longer lived radionuclides.[1] DGR is a multi-barrier system to deposit radioactive waste, mainly generated by nuclear industry. A DGR option is to encapsulate the nuclear waste in metal containers (steel, iron, copper, etc.) surrounded by compacted bentonites, considered as geotechnical barriers, and emplace them in a stable geological formation at about 500-1000 m depth.[2] A high microbial diversity in bentonite clay formations from Almeria (Spain), considered as reference material of engineered barriers for repositories, has been previously reported.[3,4] Several studies have evidenced the impact of microbial processes on the corrosion of metal containers (steel, iron, copper, etc.), which could lead to the release of radionuclides to the surrounding environment.[5] Microbial processes also seem to play a crucial role controlling the speciation and mobility of radionuclides present in radioactive wastes, such as uranium (U) and curium (Cm).[3,4,6] Therefore, understanding the migration behavior and the environmental fate of radionuclides influenced by microorganisms will be essential for the risk assessment of repositories. Cm is a highly toxic radionuclide as indicated by the high α activity of some isotopes, such as $^{247}$Cm (half-life: 1.6 x $10^7$ years) and $^{248}$Cm (half-life: 3.5 x $10^6$ years) present in nuclear spent fuel.[7,8] Cm is a representative of trivalent actinides ($An^{III}$), which exhibits excellent luminescence properties that make it suitable for direct speciation studies at environmentally relevant metal concentration.[9] Similarly, europium (Eu) has been

studied as an inactive analogue of $An^{III}$, also providing excellent luminescence properties.[10]

Among other mechanisms, microbes can interact with actinides and lanthanides through the biosorption at cell surfaces.[11] A number of functional groups (*e.g.* carboxyl, phosphoryl) on microbial surfaces have been described to be effective for actinide complexation.[12,13] $Cm^{III}$ and $Eu^{III}$ form strong complexes with phosphoryl and carboxyl sites of the bacterial cell wall of *Sporomusa* sp. MT-2.99 and *Pseudomonas fluorescens.*[12,14] Recently, Yeasts and Archaea have also been investigated for their ability to complex $An^{III}$ (*e.g.* Cm) and trivalent lanthanides ($Ln^{III}$) (*e.g.* Eu) through carboxyl and phosphate groups.[15,16] In addition, biofilm formation by microorganisms has to be considered, as it could lead to the immobilization of bioabsorbed radionuclides within the DGR system and consequently, could affect their integrity.

Since cell surfaces play a major role in the complexation of $Cm^{III}$ and $Eu^{III}$, different spectroscopic and microscopic techniques can be used to investigate the contribution of functional groups and the corresponding mechanisms involved in the biosorption of these elements. Attenuated total reflection-Fourier transform infrared (ATR-FTIR) spectroscopy, X-ray photoelectron spectroscopy (XPS), and time-resolved laser-induced fluorescence spectroscopy (TRLFS) are useful spectroscopic tools to determine the chemical speciation of these elements at environmentally relevant conditions. Potentiometric titrations have been used to determine types and abundance of active metal binding sites at the cell surface.[17,18] While a multidisciplinary approach combining different microscopic, spectroscopic, and potentiometric titration based methods is usually applied to investigate the interactions of U, as hexavalent actinide, with microbes,[13,19] the microbial interactions with Cm and Eu have only covered the use of TRLFS and potentiometric techniques.[12,14]

Spanish bentonite clays (Almeria, Spain) have shown to be excellent and suitable reference material of engineered barriers for DGRs due to their physico-chemical properties (low permeability, plasticity, high swelling pressure, thermal conductivity, etc.).[4] From these clays, *Stenotrophomonas bentonitica* has been isolated and well characterised,[20] and shown to influence the chemical speciation and mobility of other elements present in radioactive waste such as selenite ($Se^{IV}$) and $U^{VI}$.[4,21] However, the interactions between $Eu^{III}$/$Cm^{III}$ and *S. bentonitica* have never been described before. For all mentioned above, the use of this strain as a model bentonite bacterial strain to investigate the impact of bentonite microbial population in the speciation of radionuclides within the concept of DGR is novel and could provide interesting results with regard to the biological, chemical and physical analysis that are currently undergoing to evaluate the DGR safety.

The present work studies the effect of *S. bentonitica* on the environmental fate of $Eu^{III}$ and $Cm^{III}$ under aerobic and anaerobic conditions, analogous to those expected in the geodisposal of radioactive waste. For this purpose, a combination of spectroscopic (ATR-FTIR, XPS, TRLFS) and microscopic (STEM-HAADF: Scanning Transmission Electron Microscopy-High Angle Annular Dark Field) techniques have been employed. This study will provide new insights on the influence of bentonite bacterial isolates in the immobilization of $An^{III}$ within the concept of radioactive waste disposal, and will be useful to compare with other studies using elements such as Se and U. The safety of the DGR system have been well studied from a geological, chemical, and physical point of view, but not many studies have been conducted on the influence of microbiology. Therefore, this work is crucial to better understand how microbes can affect the safety of the disposal of such residues, which is a major environmental problem nowadays.

## 3. Materials and Methods

Experimental procedures related to preparation of $Eu^{III}$ and $Cm^{III}$ stock solutions, potentiometric titration of cell surfaces of *S. bentonitica* treated with $Eu^{III}$, $Eu^{III}$ biosorption experiments, TRLFS experimental setup, and STEM-HAADF analysis are provided in the Supporting Information. Due to the hazardous nature and difficult handling of $Cm^{III}$, proper safety precautions and methodologies were employed in this study.

### 3.1. Bacterial strain and growth conditions

The bacterial strain used was isolated from bentonite clay formations recovered from Almeria (Spain),[4] and was recently described as a novel species named *Stenotrophomonas bentonitica* BII-R7$^{T}$.[22] The cells were grown aerobically in Luria-Bertani (LB) broth medium (tryptone 10 g/L, yeast extract 5 g/L and NaCl 10 g/L, pH 7.0 ± 0.2) at 28 ºC under agitation (180 rpm).

### 3.2. Attenuated total reflection-Fourier transform infrared (ATR-FTIR) spectroscopy

*S. bentonitica* cells were suspended in a 30 µM $Eu^{III}$ chloride solution ($EuCl_3 \cdot 6H_2O$) under aerobic conditions at pH 6. After 48 hours, the samples were collected by centrifugation (2700 x g; 10 min) and washed with 0.1 M $NaClO_4$. Finally the samples were lyophilized according to standard protocols.[17,23] Bacterial cells without addition of $Eu^{III}$ were employed as controls.

ATR-FTIR measurements were performed on a Perkin Elmer Spectrum Two spectrometer, equipped with an ATR accessory, consisting of a diamond crystal at a fixed angle of 45º. 32 scans with spectral resolution 4 $cm^{-1}$ and wavenumber range from

4000 to 400 $cm^{-1}$ were collected for each sample. All measurements were performed in triplicate.

3.3. X-ray photoelectron spectroscopy (XPS)

$Eu^{III}$-treated cells of *S. bentonitica* were prepared as described in the section 1.3 of the Supporting Information. The obtained powder was mounted on standard sample studs using double-sided adhesive tape. Non-treated cells were prepared and used as controls. XPS measurements were made on a KRATOS SUPRA Photoelectron Spectrometer at 10 KV and 20 mA using a monochromatic Al Kα X-ray source (1486.6 eV). The take-off angle was fixed at 90º. On each sample the data were collected from three randomly selected locations, and the area corresponding to each acquisition was 400 μm in diameter. Each analysis consisted of a wide survey scan (pass energy 160 eV, 1.0 eV step size) and high-resolution scan (pass energy 20 eV, 0.1 eV step size) for component speciation. All experiments were conducted in triplicate. The binding energies of the peaks were determined using the $C_{1s}$ peak at 284.5 eV. The software CasaXPS 2.3.17 was used to fit the XPS spectra peaks.[24]

3.4. Time-resolved laser-induced fluorescence spectroscopy (TRLFS) analyses

TRLFS measurements were performed in order to determine $Eu^{III}$/$Cm^{III}$ species involved in interactions with the bacterial cells. Cells of *S. bentonitica* were brought into contact with 30 μM $Eu^{III}$ both aerobically and anaerobically and with 0.3 μM $Cm^{III}$ anaerobically, and collected as indicated in section 1.3 of the Supporting Information. The inactivity and hence easy handling of $Eu^{III}$ allowed the TRLFS studies under both respiring conditions. The $Cm^{III}$ experiments were performed anaerobically in a glove box in order to exclude carbonate complexation of $Cm^{III}$ and for radiation protection

171 issues. The obtained pellets were washed and subsequently re-suspended in 5 mL of 0.1
172 M $NaClO_4$ for analysis by TRLFS. For $Eu^{III}$, the pH was kept constant at 6, while
173 varying the incubation time (1, 24 and 48 h). For $Cm^{III}$, a pH dependent spectroscopic
174 titration (pH 2.33 to 8.04) was carried out.
175
176 **4. Results and discussion**
177 4.1. Potentiometric titration studies
178 The potentiometric titrations curves of *S. bentonitica* BII-R7 before and after $Eu^{III}$
179 exposure are presented in Figure S1. The concentration of deprotonated sites is
180 standardized per mass of dry biomass (mol $g^{-1}$), and calculated according to Fein et al.[25]
181 To calculate the acidity constants and the total concentration of each binding site, data
182 from the titrations curves were fitted using ProtoFit 2.1 rev1,[26] using a Non-
183 Electrostatic Model (NEM). It has been demonstrated that electrostatic treatments, such
184 as diffuse layer and triple layer electrostatic models to titration data, greatly over-predict
185 the effect of ionic strength on bacterial surface protonation reactions, resulting in poorer
186 fits and more variability in stability constants than non-electrostatic models.[27,28]
187
188 The titrated bacterial suspensions exhibited a protonation-deprotonation behaviour over
189 the whole pH range studied (Figure S1). The shape of the titrations curves obtained
190 suggested the presence of functional groups with close acid-base $pK_a$ values, showing
191 that although some small variability could be perceived in each set of the same bacterial
192 sample, essentially reproducible results were obtained (the variation between the
193 titration curves was below 6% of $[H^+]_{exchanged}$ between pH 3.5 and 10.0). Although a
194 small hysteresis could be observed between acid and base titrations at the same ionic

195 strength, results from reverse titrations did not vary strongly and suggested a reversible
196 proton adsorption/desorption reaction.
197 Table S1 summarizes the $pK_a$ values for *S. bentonitica* before and after $Eu^{III}$ exposure.
198 The calculated values were 4.97 ± 0.08 and 4.78 ± 0.06 for $pK_1$, 6.88 ± 0.02 and 6.75 ±
199 0.13 for $pK_2$, and 9.43 ± 0.02 and 9.48 ± 0.11 for $pK_3$. The obtained $pK_a$ values are
200 representative of carboxylic groups for $pK_1$, phosphate groups for $pK_2$ and amine and
201 hydroxyl groups for $pK_3$.[17,18,25,29–32]
202 The existence of pH zero proton charge ($pH_{zpc}$) indicated that *S. bentonitica* developed a
203 positive net charge at low pH values, indicating the presence of at least one positively
204 ionising, plausibly amino group. Models which only include negatively ionising groups
205 such as carboxyl, phosphoryl and hydroxyl groups could not develop a net positive
206 charge at low pH.[33] The $pH_{zpc}$ around 5.7 also indicated that the cells were negatively
207 charged at neutral pH = 7 and electrostatic attraction with positive-charged mineral
208 surfaces or metals is favourable.
209 The surface site densities obtained using ProtoFit are also presented in Table S1. The
210 $pK_a$ values for bacterial samples with and without $Eu^{III}$ were comparable, indicating
211 similar concentration of the active functional groups on the cell wall. One exception
212 was found, the concentrations corresponding to phosphate groups ($C_2$) was significantly
213 lower for *S. bentonitica* cells exposed to $Eu^{III}$. This could suggest a strong affinity of
214 $Eu^{III}$ to phosphate sites, making them inaccessible to the protonation/deprotonation
215 reaction. The considerable high concentration of phosphate groups at the surface of *S.*
216 *bentonitica* (10.78 ± 0.31 x $10^{-4}$ mol/g) comparing with other bacterial species such as
217 *Sporomusa* sp. MT-2.99 (5.30 ± 0.8 x $10^{-4}$ mol/g), *Sphingomonas* sp. S15-S1 (3.16 ±
218 0.56 x $10^{-4}$ mol/g), or *B. sphaericus* JG-7B (2.19 ± 0.25 x $10^{-4}$ mol/g)[12,34] (Table S1)
219 pointed out the potentially high metal-binding ability of *S. bentonitica*.

The results of potentiometric titration experiments indicated that the cell surface groups capable for metal binding sites could involve carboxyl groups (pK around 3-5), phosphate groups (pK around 6-7), and hydroxyl and amine groups (pK > 8). These findings are in agreement with previous studies on bacterial surfaces.[17,35,36] Liu et al.[36] demonstrated the role of carboxyl, phosphoryl, and amino functional groups of *Synechococcus* sp. PCC 7002 cells as metal surface ligands by means of potentiometric titrations. In the case of $Eu^{III}$ and $Cm^{III}$, their sorption on the cell envelope of *Sporomusa* sp. MT-2.99, *B. subtilis* and *P. fluorescens* can be due to their coordination with carboxyl and phosphate groups.[12,14,37,38] Consequently, phosphate and carboxyl groups of *S. bentonitica* might be expected to be involved in the binding of $Eu^{III}$. However, the potentiometric results only showed phosphate groups as the main potential binding sites in the pH range studied due to their high surface concentration. It is probable that the extent of the carboxyl group involvement in the $Eu^{III}$ binding is either too small to be detected by titration methods, or the sorption/desorption of $Eu^{III}$ by the carboxylic groups is reversible at low pH (possible exchange between Eu(III) and protons at low pH for the carboxylate groups).

4.2. $Eu^{III}$ removal capacity of *S. bentonitica* over time

These studies were carried out to estimate the $Eu^{III}$ removal capacity of *S. bentonitica* with increasing time under aerobic and anaerobic conditions. The maximum amount of $Eu^{III}$ removal was 12.9 ± 0.11 mg of Eu/g of dry biomass after 96 h of aerobic incubation (Figure S2). This amount corresponds to a 54 ± 0.44 % of $Eu^{III}$ removed from the total amount of Eu in the solution. Higher values were obtained by Bader et al. (2019)[16] in their bioassociation kinetics studies with the halophilic archaeon *Halobacterium noricense* DSM15987$^T$ by using the same $Eu^{III}$ initial concentration (30

μM). They found that around 73% of $Eu^{III}$ was removed after 1 week of incubation. Under anaerobic conditions, the maximum amount of $Eu^{III}$ removal was 6.06 ± 0.25 mg of Eu/g of dry biomass after 18 h incubation (Figure S2), which corresponds to a 31.2 ± 1.3 % of $Eu^{III}$ removal. The $Eu^{III}$ removal improved by increasing contact time of incubation until equilibrium was attained under both conditions. However, these results clearly showed that *S. bentonitica* cells have a higher removal capacity under aerobic conditions. This could be a consequence of the more stressful anoxic conditions, probably affecting the bacterial interaction process.

These results suggested that the interaction was mediated not only by biosorption, since this mechanism is generally defined as a quick process ocurring up to a few hours.[39] More specifically, the $Eu^{III}$ removal studies showed that time-dependent Eu interaction with the cells could be a biphasic process. First, a rapid phase where 12.5 ± 0.73 and 13.9 ± 1 % of $Eu^{III}$ removal was achieved (aerobically and anaerobically, respectively) within the first 2 h (Figure S2). This fast phase is usually associated to metabolic independent biosorption mechanisms. Secondly, a slow phase seems to occur, where $Eu^{III}$ accumulation process seems to reach equilibrium after 24 h. This phase could be controled by metabolically dependent interaction mechanisms such as intracellular accumulation or bioprecipitation, among others.

### 4.3. Characterization of $Eu^{III}$-*S. bentonitica* interactions using ATR-FTIR

Figure 1 shows the ATR-FTIR spectra obtained from *S. bentonitica* after 48 h incubation with 30 μM $Eu^{III}$ solution. The observed infrared bands confirmed the presence of proteins, lipids, polysaccharides, and polyphosphate groups. The functional groups assigned to the infrared bands and the corresponding frequencies for the bacterial cells are summarised in Table S2.

The region between 3000 and 2800 $cm^{-1}$ exhibited the typical C-H stretching vibrations ($\nu_{C-H}$) corresponding to the $CH_3$ and $>CH_2$ functional groups present in the fatty acids and lipids, and the O-H stretching band ($\nu_{O-H}$) corresponding to the presence of hydroxyl groups in bacterial cells. Complementary information could be found at the region between 1800 and 750 $cm^{-1}$, where vibrations of C-H, $>CH_2$ and $-CH_3$ groups, amides, carbonyl groups and polysaccharides were observed. The peaks observed at 1308 and 1455 $cm^{-1}$ could be attributed to the bending of $-CH_3$ and $>CH_2$ of proteins ($\delta_{CH2}$, $\delta_{CH3}$), and the signals at 1635 and 1535 $cm^{-1}$ corresponded to the amide I and II bands, respectively. The amide I band was due to the stretching C=O ($\nu_{C=O}$) of amides associated with proteins and the amide II band was actually a combination of bending N-H ($\delta_{N-H}$) of amides and contributions from stretching C-N ($\nu_{C-N}$) groups. The peak at 1455 $cm^{-1}$ also concealed the amine III group. The peak around 1404 $cm^{-1}$ was due to the symmetric stretching C-O of carboxylate groups ($\nu_{sym\ COO^-}$), and the peak corresponding to the asymmetric stretching vibration ($\nu_{asym\ COO^-}$) was concealed by the amide II band at 1535 $cm^{-1}$. A small shoulder around 1745 $cm^{-1}$ was a combination of two peaks: a signal corresponding to the vibrational C=O stretching ($\nu_{C=O}$) of carboxylic acids at 1747 $cm^{-1}$ and another peak corresponding to the stretching C=O of ester functional groups from membrane lipids and fatty acids at 1730 $cm^{-1}$.[17,30,31,40] The double bond stretching of >P=O of general phosphoryl groups and phosphodiester of nucleic acids could be observed at 1240 $cm^{-1}$. The stretching of P=O groups of polyphosphate products, nucleic acid phosphodiester and phosphorylated proteins can be found around 1070 $cm^{-1}$, and the peak at 933 $cm^{-1}$ showed the asymmetric O-P-O stretching modes.[30,31,40]

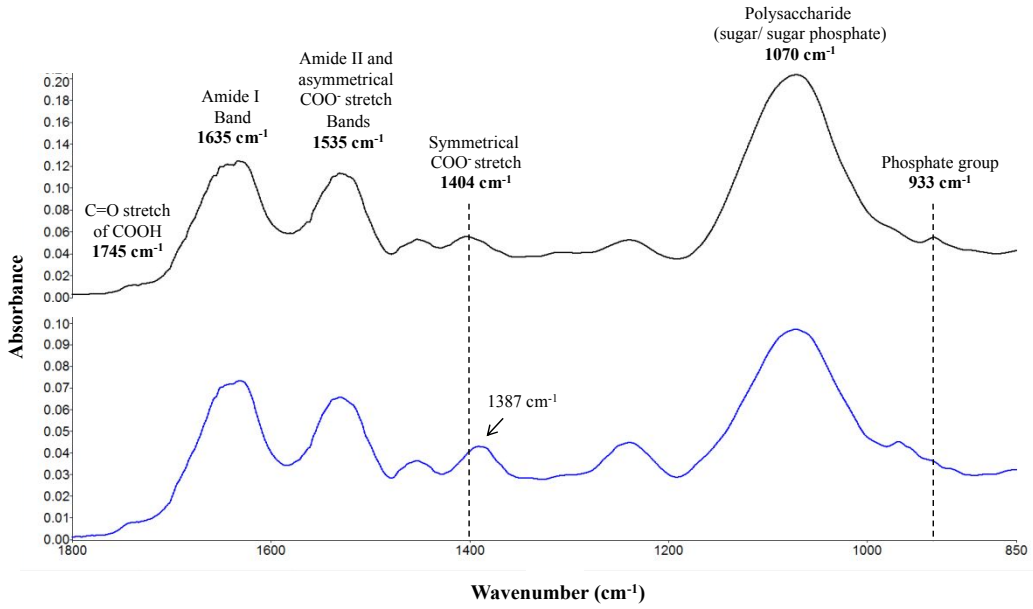


**Figure 1.** Comparison between the ATR-FTIR spectra for *S. bentonitica* cell suspensions in 0.1 M $NaClO_4$ (electrolyte) solution only (top, in black color) and in 30 μM $Eu^{III}$ solution + electrolyte (bottom, in blue color) after 48 hours.

The ATR-FTIR spectra showed a shift in the band attributed to symmetric stretching of carboxylate groups (around 1404 $cm^{-1}$) to lower frequencies, when compared to the spectra of the cells in background electrolyte (Figure 1). Extensive studies made on metal complexes of carboxylic acids have established an empirical correlation between the position of the symmetric stretching ($\nu_{sym\ COO^-}$) and asymmetric stretching ($\nu_{asym\ COO}$) of carboxylate groups and the difference in frequency between them ($\Delta\nu$). The values of $\Delta\nu$ descend in the follow order: $\Delta\nu_{unidentate} > \Delta\nu_{brinding} \sim \Delta\nu_{free\ ionic} > \Delta\nu_{chelate(bidentate)}$.[41–44] Chu et al.[41] and Deacon and Phillips,[44] after careful examinations of IR spectra of many acetates with known X-ray crystal structures, arrived at the conclusion that: i) for unidentates complexes, $\Delta\nu > 200$ $cm^{-1}$ and the position of $\nu_{sym\ COO^-}$ is generally shifted to lower frequencies; ii) for bidentate chelating complexes, $\Delta\nu < 100$ $cm^{-1}$ and the position of $\nu_{sym\ COO^-}$ is shifted to higher frequencies, whereas $\nu_{asym\ COO^-}$ is shifted to

lower frequencies; and iii) for bidentate bridging complexes, $\Delta\nu \sim 160$ cm$^{-1}$ and the position of $\nu_{sym\ COO^-}$ and $\nu_{asym\ COO^-}$ can shift in either direction.[41] The symmetric stretching ($\nu_{sym\ COO^-}$) band for *S. bentonitica* in contact with $Eu^{III}$ shifted to lower frequencies by ~15 cm$^{-1}$, but, as can be observed in Figure 1 and Table S2, the asymmetric stretching ($\nu_{asym}$ $COO^-$) of carboxylate groups was hidden by the amide II band, and therefore it is difficult to determine if there was a shift in this band to higher or lower frequencies. Based purely on the position of $\nu_{sym\ COO^-}$ shifting to lower frequencies, the carboxyl functional groups could form unidentate complexes with the $Eu^{III}$ metals. If the asymmetric stretching ($\nu_{asym\ COO^-}$) of carboxylate groups (hidden by the amide II band) did not shift, then $\Delta\nu$ would be around 150 cm$^{-1}$, suggesting that the carboxyl functional groups arising from the macromolecules of the cell wall of the bacterial cells could form bidentate bridging complexes with the $Eu^{III}$ metals. However, further studies would be needed as there is no evidence of the frequency of the asymmetric $\nu(COO^-)$ mode. EXAFS analysis could provide more detailed information about the local coordination of Eu associated with these cells, but it falls beyond the main scope of this study. This would provide more unequivocal indications of the ability of bentonite-isolated bacteria to interact with Eu in a unidentate or bidentate bridging mode. Nevertheless, these results provide further verification that carboxyl functional groups from the macromolecues of the bacterial cells are responsible in forming organo-metallic complexes with the $Eu^{III}$ metals, as also reported by the potentiometric and luminiscence results.

In addition, the ATR-FTIR spectra indicated that phospholipids might also be involved in the cell-metal complexation. The lower intensity of the band found at 933 cm$^{-1}$ of $Eu^{III}$-treated cells compare with $Eu^{III}$-untreated cells suggests phosphate groups as candidates for $Eu^{III}$ complexation.[23]

335 4.4. Characterization of $Eu^{III}$-*S. bentonitica* interactions using XPS.

336 This method was applied to determine the local coordination of $Eu^{III}$ at the cell surface
337 of *S. bentonitica* approximately up to 5 nm.[45] The elemental composition of the *S.*
338 *bentonitica* surface, resulting from integrating the $C_{1s}$, $O_{1s}$, $N_{1s}$ and $P_{2p}$ from the wide
339 scan spectrum can be seen in Figure 2A-D. Sodium and chlorine were also detected as
340 samples were washed with 0.1 M $NaClO_4$. Eu was detected in the bacterial sample in
341 contact with a 30 μM $Eu^{III}$ solution for 48 hours. Nitrogen appeared at a binding energy
342 of 399.99 eV, attributable to amine or amide groups of proteins.[23,46–49] Phosphorus was
343 found at a binding energy of 133.99 eV, and can be attributed to phosphate groups.[47–49]
344 The presence of amine groups from proteins and phosphate groups based on the binding
345 energies of $N_{1s}$ and $P_{2p}$ are in agreement with the results from potentiometric titrations
346 ($pK_a$ = 6.8 and $pK_a$ = 9.4) and the FTIR spectra (adsorption bands at 1635 $cm^{-1}$, 1535
347 $cm^{-1}$, and 933 $cm^{-1}$).

348 XPS peaks corresponding to $Eu_{3d}$ were also analysed at high resolution to assess the
349 nature of the $Eu^{III}$ complex and shown in Figure 2D. The local coordination of Eu
350 associated to the cells of the studied strain, observed at 1135 eV, is similar to that of Eu-
351 acetate as was described by Mercier et al.[50] This suggests that carboxyl groups
352 containing cell wall molecules like glutamic acid of peptidoglycan are involved in the
353 Eu binding. Previous studies showed the role of carboxyl groups from glutamic and
354 aspartic acid present in proteins of the S-layer of *B. sphaericus* in the complexation of
355 uranium and palladium.[51,52] Therefore, carboxyl groups of the glutamic acid of the
356 peptidoglycan (PG) layer of *S. bentonitica* could be involved in the interaction of $Eu^{III}$.

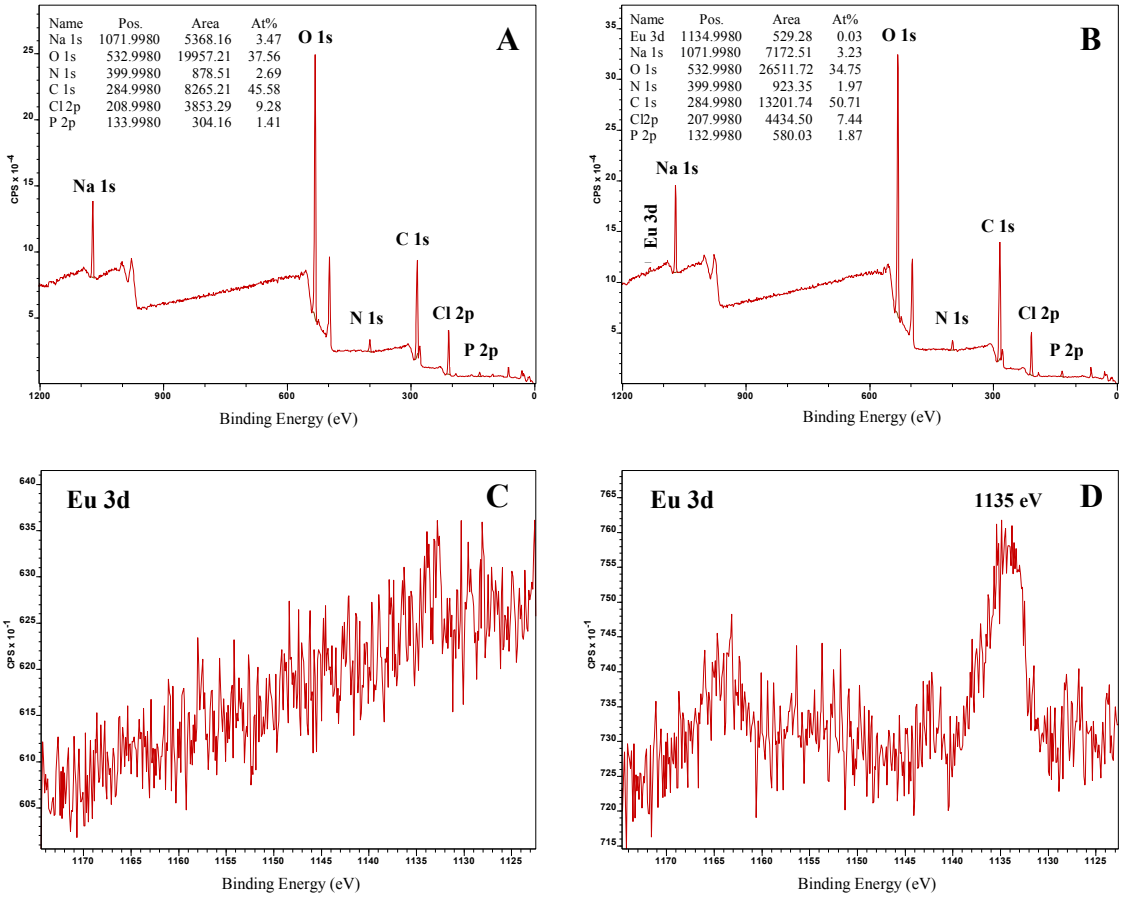


**Figure 2.** XPS spectra of *S. bentonitica* in absence (A, C) and presence of 30 µM $Eu^{III}$ (B, D). High-resolution spectra of the region belonging to Eu 3d (C and D).

4.5. TRLFS characterization of $Eu^{III}$/$Cm^{III}$ interaction with *S. bentonitica*

Potentiometric titrations, ATR-FTIR, and XPS studies showed the involvement of phosphate and carboxyl groups in the coordination of $Eu^{III}$ by the *S. bentonitica* cells. In addition, $Eu^{III}$ and $Cm^{III}$ were used as luminescence probes to investigate $Cm^{III}$/$Eu^{III}$ binding on *S. bentonitica* based on changes of the intrinsic luminescence properties due to microbial interaction. The studies with $Cm^{III}$, radioactive analogue of $Eu^{III}$, were carried out at much lower concentrations relevant to environmental conditions (0.3 µM).

370 *4.5.1. Europium*

371 The luminescence spectra depicted in Figure 3 showed the interaction of $Eu^{III}$ with *S.*
372 *bentonitica* through typical changes as result of cell addition after 1, 24 and 48 h of
373 anaerobic incubation at pH 6 in both, supernatants and re-suspended cells. This
374 suggested the complexation of $Eu^{III}$ with extracellular released complexing agents and
375 bacterial surface functional groups, respectively. In the supernatant and the re-
376 suspended cells the $^7F_0$ transition appeared at 579 nm with a slightly higher intensity
377 than in the blank sample. This pointed to a different symmetry around the $Eu^{III}$ center
378 compared to the blank spectrum and is a further argument for interaction process of
379 $Eu^{III}$ with the cells. The luminescence spectrum of $Eu^{III}$ aqua ion (blank) is
380 characterized by emission bands at 585-600 nm (magnetic dipole transition $^5D_0 \rightarrow {}^7F_1$)
381 and 610-630 nm (hypersensitive transition $^5D_0 \rightarrow {}^7F_2$). An increased intensity of the
382 hypersensitive $^7F_2$ transition at 617 nm moving from blank via supernatant to the re-
383 suspended cells was discovered.

384 In the supernatants, there was a systematic increase in the $^7F_2$ transition as a function of
385 the incubation time (Figure 3A). This could indicate an increase in the release of
386 complexing agents from the cells at a longer incubation time. Total organic carbon
387 (TOC) content of the supernatant samples increased after 24 h of incubation (Figure
388 S3), suggesting the release of complexing substances from the cells. These results are in
389 agreement with the $Eu^{III}$ removal studies (section 4.2), in which the amount of Eu
390 adsorbed increased with the incubation time. In the re-suspended cells, there was a fast
391 rise in the intensity of the $^7F_2$ transition after an incubation time of 1 h. Then, no
392 systematic changes in the spectra, as a function of the incubation time, were observed
393 (Figure 3B).

394

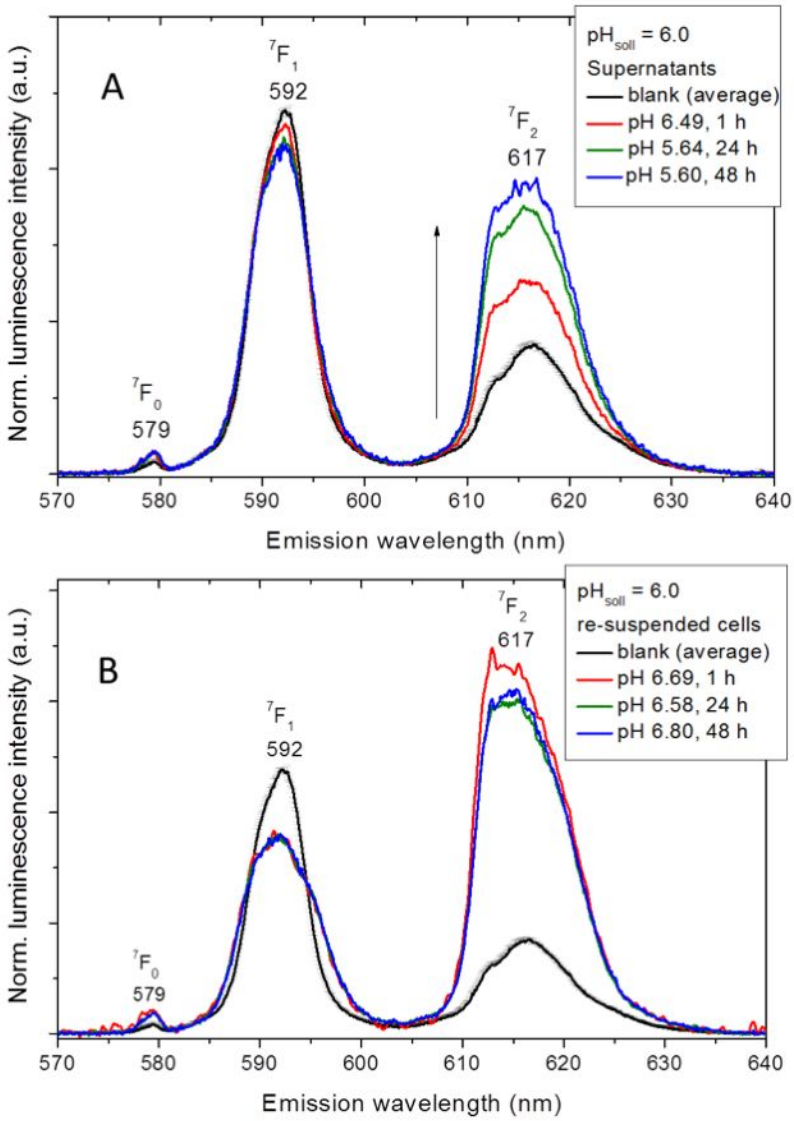


395

396 **Figure 3.** Luminescence emission spectra of 30 µM $Eu^{III}$ measured for the supernatants
397 after separating the *S. bentonitica* cells (0.2 g/L) (A) and the re-suspended cells (B)
398 under anaerobic conditions at pH 6 and different incubation times (1, 24 and 48 hours)
399 in 1 M $NaClO_4$.

400

401 In supernatants and re-suspended cells, $Eu^{III}$ appeared in two different coordination
402 environments. The short-lived component in supernatants was measured at 117, 129 and
403 133 µs after 1, 24, and 48 h, respectively (Table 1). These lifetimes indicated a similar

coordination environment after 24 and 48 h. Those $Eu^{III}$-species containing approximately eight water molecules and one binding site will be filled by functionalities of the released substances. The luminescence lifetime of 114 ± 5 µs corresponding to 8.8 ± 0.5 coordinated water molecules found in the blank was characteristic to the $Eu^{3+}$ ion. The short lifetime of 117 µs found in the supernatant after 1 h of incubation indicated the presence of the $Eu^{III}$ ion. The longer lifetimes, 387 to 500 µs, could indicate an interaction of $Eu^{III}$ with released substances from the cells independently from the incubation time. In this second type of $Eu^{III}$ complex only up to 1 to 2 water molecules remained. In the case of re-suspended cells, a bi-exponential luminescence decay was measured indicating two coordination environments of $Eu^{III}$. The short-lived component showed luminescence lifetimes between 144 and 225 µs (7 and 4 coordinated water molecules, respectively), whereas the long-lived component varied between 477 and 609 µs (2 and 1 coordinated water molecules, respectively). In a first approximation, similar $Eu^{III}$ species were formed for the short-lived component of the supernatant and re-suspended cells. In the same way, the long-lived component of both supernatant and re-suspended cells suggested a similar coordination environment but different from the one found for the short-lived component.

By comparing our lifetime results with literature data, phosphoryl and carboxyl groups present on bacterial cell envelopes and bacterial released substances seem to play an important role in the $Eu^{III}$ coordination sites characterized by, for instance, their individual luminescence lifetimes, probably in form of R-O-$PO_3$-$Eu^{2+}$ (R-O-$PO_3$H-$Eu^{2+}$ under acidic pH conditions) and R-COO-$Eu^{2+}$ as revealed by previous studies (Table 1).[12,53] Specifically, the $Eu^{III}$-*S. bentonitica* complexes seem to have similar properties as the surface species R-O-$PO_3$H-$Eu^{2+}$observed on cell envelopes of *Sporomusa* sp. MT-2.99 as revealed by the long lifetimes.[12] The coordination site characterized by

429 short lifetimes seem to interact with $Eu^{III}$ with similar properties as the surface species
430 R-COO-$Eu^{2+}$ observed on cell envelopes of *Sporomusa* sp. MT-2.99 and *P.*
431 *fluorescence.*[12] It is important to note that the results presented here were very similar to
432 those obtained aerobically and have comparable significance (Figure S4).
433

434 **Table 1.** Spectroscopic properties obtained from the $Eu^{III}$-*S. bentonitica* system at pH 6
435 using different incubation times and other relevant model systems.

| **Sample** | **$R_{E/M}$** | **Lifetime (µs)** | **Proposed species** | **Reference** |
|---|---|---|---|---|
| **$Eu^{III}$ control** | 0.50 ± 0.05 | 114 ± 5 | $Eu^{3+}$ | This work |
| **Supernatants** | | | | This work |
| **$Eu^{III}$-*S. bentonitica*** | | | | |
| 1 h incubation | 0.9 | 117; 387 | $Eu^{3+}$; phosphoryl sites | |
| 24 h incubation | 1.2 | 129; 490 | Carboxyl; phosphoryl | |
| 48 h incubation | 1.3 | 133; 500 | Carboxyl; phosphoryl | |
| **Cells** | | | | This work |
| **$Eu^{III}$-*S. bentonitica*** | | | | |

| | | | | |
|---|---|---|---|---|
| 1 h incubation | 2.3 | 144; 477 | Carboxyl; phosphoryl sites | |
| 24 h incubation | 2.1 | 174; 561 | Carboxyl; phosphoryl | |
| 48 h incubation | 2.1 | 225; 609 | Carboxyl; phosphoryl | |
| **$Eu^{III}$-*Sporomusa* sp. MT-2.99** | 3.3 | 170 | R-COO-$Eu^{2+}$ | Moll et al.[12] |
| | 1.8 | 515 | R-O-$PO_3H$-$Eu^{2+}$ | |
| **$Eu^{III}$-*Bacillus subtilis*** | | 230 | Carboxyl sites | Markai et al.[54] |
| | | 730 | Phosphoryl sites | |
| **$Eu^{III}$-*Pseudomonas aeruginosa*** | | 98-254 | Carboxyl sites | Texier et al.[53] |
| | | 534-677 | Phosphoryl sites | |

436

437 *4.5.2. Curium*

438 The chemical speciation of $Cm^{III}$ with *S. bentonitica* cells was studied at trace (0.3 μM)
439 $Cm^{III}$ concentrations by TRLFS. These measurements were conducted assuming that the
440 influence of the luminescence properties of the microbial $Cm^{III}$-species dominates over
441 the influence of soluble $Cm^{III}$-species with, for instance, released complexing agents.

442 The pH-dependent spectroscopic $Cm^{III}$ speciation in the cell suspensions is shown in
443 Figure 4.

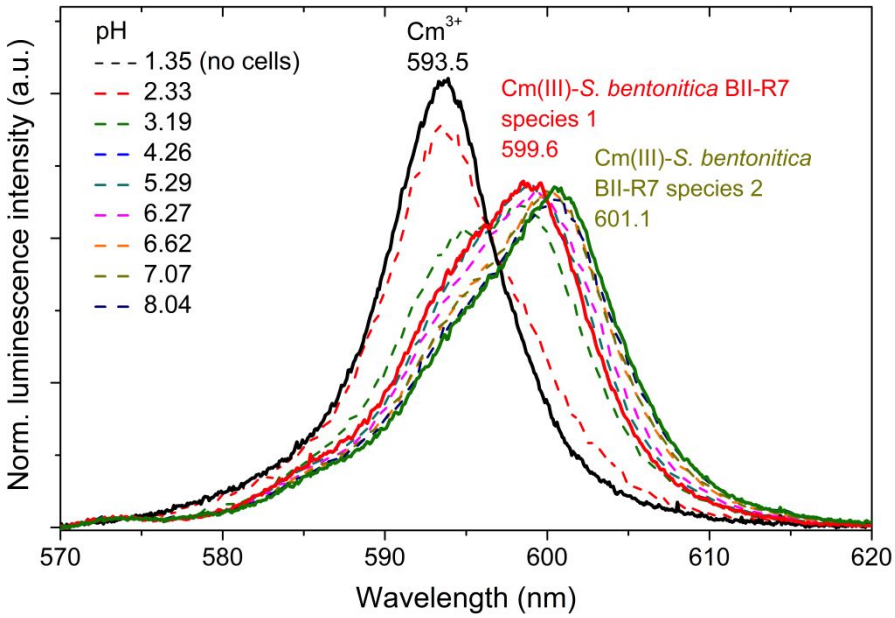


444

445 **Figure 4.** Luminescence emission spectra of 0.3 µM $Cm^{III}$ in 0.1M $NaClO_4$ measured as
446 a function of pH at a fixed biomass concentration of 0.2 $g_{dry\ weight}$/L.

447

448 From the dependencies found in the TRLFS spectra, it can be concluded that there are
449 two coordination environments of $Cm^{III}$ due to interactions with functional groups of
450 the cell surface and possibly with released complexing agents. Thus, the Hypspec
451 analysis of the pH dependent emission spectra measurements revealed two $Cm^{III}$
452 bacterial species (Figure 4). $Cm^{III}$-*S. bentonitica* species 1 was characterized by an
453 emission maximum at 599.6 nm while $Cm^{III}$-*S. bentonitica* species 2 showed a more red
454 shifted emission maximum at 601.1 nm. The extracted single component spectra of both
455 species are shown in Figure 4. TRLFS of the supernatants and the $Cm^{III}$ loaded biomass
456 after washing with 0.1M $NaClO_4$ showed that 73% of the detected $Cm^{III}$ luminescence
457 intensity remained in solution at pH 8.04, while, only 23% was associated to the
458 biomass. This evidence indicated that a complexation of $Cm^{III}$ by substances released

459 from the cells was occurring. In all samples containing cells, a bi-exponential
460 luminescence decay was detected (Table S3). At pH 3.2 the short lifetime of 71 µs
461 points to uncomplexed $Cm^{3+}$. Between pH 4 and 8 both lifetimes amounted to 120 ± 8
462 and 290 ± 23 µs corresponding to 5 and 2 coordinated water molecules, respectively. By
463 comparing our results with the ones reported in literature, a close agreement was found
464 to the study of Lopez-Fernandez et al.[15] The long lifetime and the corresponding
465 emission maximum matches with $Cm^{III}$ interactions with microbial phosphoryl sites,
466 whereas the short lifetime can be attributed to carboxyl interactions of $Cm^{III}$.
467
468 4.6. Cellular localization of $Eu^{III}$ by STEM-HAADF (Scanning Transmission Electron
469 Microscopy-High Angle Annular Dark Field).
470 STEM-HAADF micrographs of thin sections of *S. bentonitica* cells exposed to $Eu^{III}$
471 revealed the presence of electron-dense accumulations, mainly at the cell surface
472 (Figure 5A-D) under both aerobic and anaerobic conditions. In addition, very few
473 extracellular (Figure 5A-D) and intracellular (Figure 5D) accumulations were observed.
474 EDX analysis (Figure 5E-F) and element-distribution mapping (Figure 6) of these
475 accumulations indicated a main composition of Eu and P. The detection of P in the
476 EDX analysis of the $Eu^{III}$ precipitates also confirmed the key role of functional groups
477 containing phosphorus in their interaction with $Eu^{III}$. These results showed biosorption
478 of $Eu^{III}$ as the main interaction mechanism with the cells of *S. bentonitica*. However, the
479 presence of few extracellular and intracellular $Eu^{III}$ precipitates indicated that the
480 interaction is not only mediated by biosorption, thus other processes, such as
481 bioaccumulation and bioprecipitation, could also occur. This matches very well with the
482 $Eu^{III}$ removal studies (section 4.2.) suggesting the implication of other interaction
483 mechanisms.

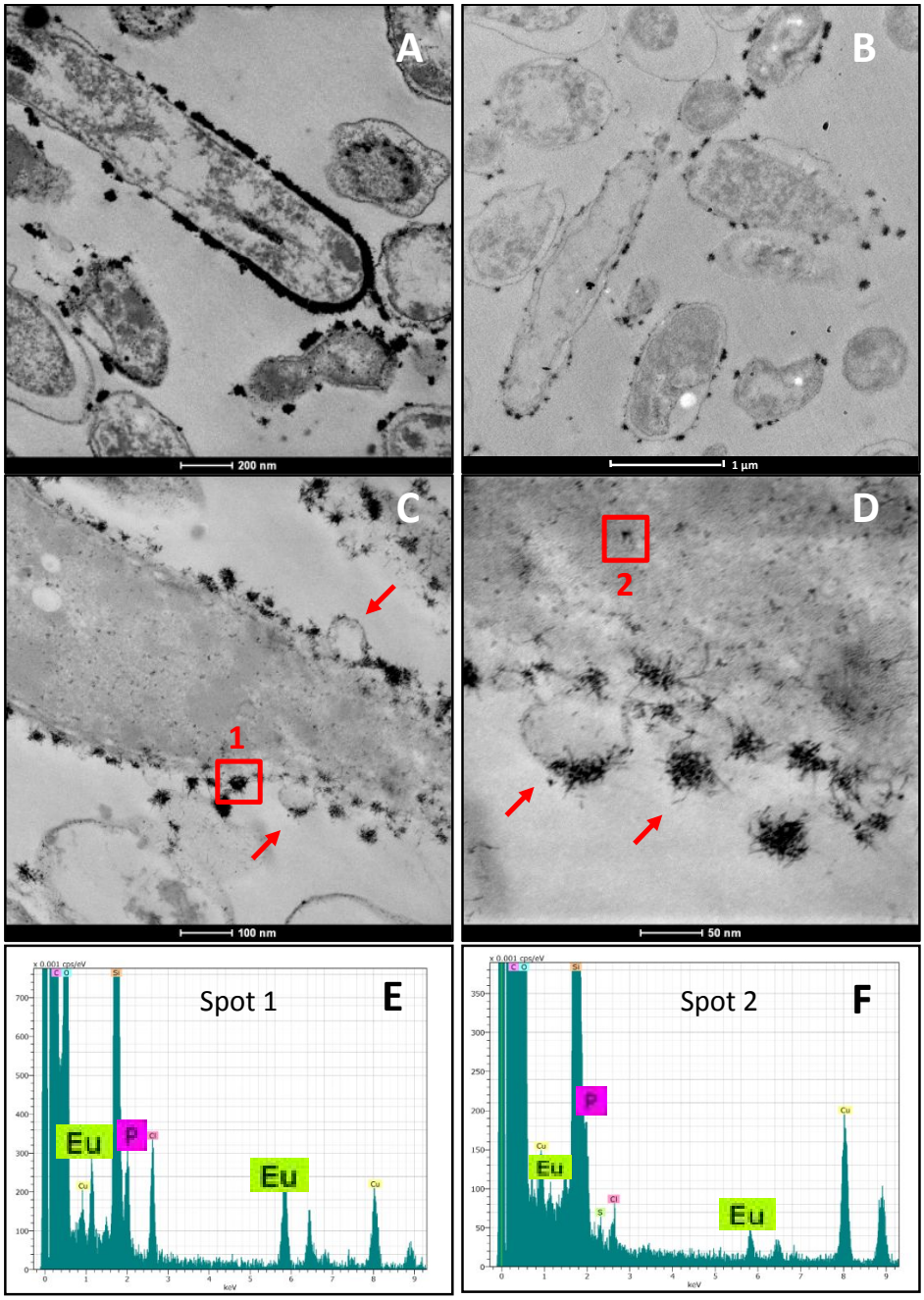


**Figure 5.** STEM-HAADF micrographs showing electron-dense accumulations at the cell surface, extracellular, and intracellularly under aerobic (A-B) and anaerobic conditions (C-D). EDX analysis (E-F) confirming the Eu and P composition of the accumulations. The formation of vesicles by *S. bentonitica* cells is indicated by arrows (C-D). Scale bars: 200 nm (A), 1µm (B), 100 nm (C), 50 nm (D).

The formation of outer membrane vesicles (OMVs) by *S. bentonitica cells* exposed to $Eu^{III}$ was observed in the STEM-HAADF micrographs (Figure 5C-D). The production of OMVs by Gram-negative bacteria plays a prominent role in cell protection against hostile environments.[55,56] Morever, it represents a mechanism to alleviate stress through the packaging and release of stress-products.[57] Therefore, the vesicle formation mechanism of *S. bentonitica* cells could be involved in their $Eu^{III}$ tolerance. In addition, the detection of extracellular precipitates could be a consequence of the release of intracellular accumulates through the formation of vesicles. However, further investigations are needed to confirm this hypothesis. On the other side, intracellullar accumulation could be a consequence of a passive process associated to damage of the cell membrane permeability, since Eu do not play any biological function and the cells do not have a specific transport system for the uptake of this element. The explanation of how and why elements such as Eu are accumulated in the cytoplasm of some microorganisms remains unknown.

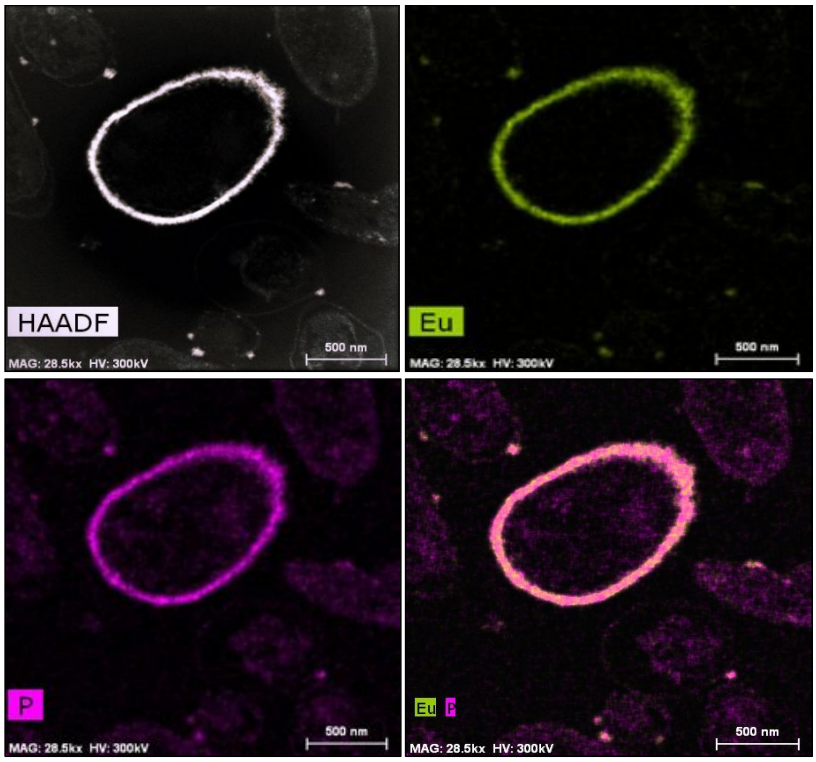


**Figure 6.** STEM-HAADF micrographs of thin sections showing the adsorption of $Eu^{III}$ on a *S. bentonitica* cell after 48 h in contact with 30 µM $Eu^{III}$ solution. Scale bars: 500 nm.

4.7. Environmental implications.

The safety of the DGR system have been well studied from a geological, chemical, and physical point of view but, very few works have investigated the impact of microbial processes in the safety of this disposal option. It is well known that microbe occurring in different DGR barriers, including bentonites, could affect the safety of a DGR through: 1) corrosion of metal containers, 2) transformation and alteration of bentonite minerals, 3) gas production, and 4) mobilization of radionuclides present in the system, such as curium, selenium, or uranium. Here we reported a clear effect of the activity of the bentonite bacterial isolate *S. bentonitica*, on the speciation and mobility of trivalent actinides such as $Cm^{III}$ and its inactive analogue $Eu^{III}$.

A multidisciplinary approach combining microscopy, spectroscopy, and potentiometric titration based methods allowed us to provide new insights on the speciation of Cm and Eu asociated with bacterial strains (isolated from one of the most important arificial barriers, bentonites, of future DGR). The results obtained revealed that carboxyl and phosporyl groups from bacterial envelopes and other extracellularly released complexing agents seem to be involved in the interaction with Eu and Cm. Specifically, XPS analysis suggested that these carboxyl groups could arise from macromolecules located at the cell surface such as glutamic acids of the peptidoglycan layer, which could be involved in the complexation of $Eu^{III}$. In addition, ATR-FTIR suggested that the coordination of $Eu^{III}$ with carboxyl groups from the bacterial cell wall could occur in a bidendate bridging mode. Finally, TEM analysis, in combination with the rest of the techniques, suggested that the Eu/Cm-bacteria interaction most probably occur through several microbial processes such as biosorption, intracellular accumulation, and biomineralization. The results here reported clearly suggested that *S. bentonitica* could influence the speciation and hence mobility of Eu and Cm, afeccting the safety of the DGR system.

Biosorption and bioaccumulation may enable the metal removal from contaminated aqueous solutions through the immobilization of bacterial biomass to inert supports,[58] which are nowadays receiving attention for bioremediation purposes. The immobilization of microorganisms in minerals from bentonites and other materials through the formation of biofilms could lead to the immobilization of bioadsorbed or bioaccumulated radionuclides. Indeed, genes coding for the formation of biofilms such as those involved in the formation of surface structures (*flhA, flhB, fliR, fliQ, fliP, fliN, fliM*) [59] or those encoding outer-membrane lipoproteins (*slp*) [60] have been reported to be

546 present in the genome of *S. bentonitica* [61] (GenBank accession number
547 MKCZ00000000). In addition, the production of flagella-like proteins by this bacterium
548 could be involved in the formation of biofilms. Clark et al.[62] demonstrated the role of
549 flagella-like filaments produced by *Desulfovibrio vulgaris* in the establishment and
550 maintenance of biofilms between cells and silica oxide surfaces. Therefore, *S.*
551 *bentonitica* could positively influence the safety of repositories by inducing the
552 immobilization of radionuclides through the biofilm formation.
553 In addition to biosorption and bioaccumulation, a long-term bioprecipitation process
554 could be involved as suggested by the extracellular Eu precipitates observed by STEM-
555 HAADF. Bioprecipitation basically leads to the inmobilization of radionuclides since it
556 is based on the conversion from soluble to insoluble forms through their precipitation
557 with released cell ligands (carbonates, phosphates, etc.).[11,63] From all mentioned above,
558 the present study could be really helpful to better understand how microbes affect the
559 safety of the disposal of radioactive residues, which is a global environmental concern
560 nowadays.
561

562 **5. Conflicts of interest**

563 The authors declare no competing financial interest.
564

565 **6. Acknowledgements**

566 This work was supported by Euratom research and training programme 2014-2018
567 under grant agreement no. 661880 and ERDF -financed Grants CGL-2012-36505,
568 CGL2014-59616-R (80% finding by FEDER). Part of this work was co-financed by the
569 European Radioecology Alliance mobility grant awarded to MAR-F. The authors
570 acknowledge the assistance of Maria del Mar Abad Ortega and Concepción Hernández

Castillo (Centro de Instrumentación Científica, University of Granada, Spain) for their help with microscopy measurements, and Dr James McGettrick (Swansea University, College of Engineering) for the help with the XPS measurements. The authors are indebted to the U.S. Department of Energy, Office of Basic Energy Sciences, for the use of $^{248}Cm$ via the transplutonium element production facilities at Oak Ridge National Laboratory; $^{248}Cm$ was made available as part of collaboration between HZDR and the Lawrence Berkeley National Laboratory (LBNL).

## 7. Supporting information

The supporting information includes 5 sections of methodology, 4 figures and 3 tables in a separate file.

1. Supplementary materials and methods

1.1. Preparation of $Eu^{III}$ and $Cm^{III}$ stock solutions

1.2. Potentiometric titration of cell surfaces of *S. bentonitica* treated with $Eu^{III}$

1.3. $Eu^{III}$ biosorption experiments

1.4. TRLFS experimental setup

1.5. STEM-HAADF analysis

2. Supplementary figures and tables

Figure S1. Representation of the potentiometric titrations of *S. bentonitica* in 0.1 M $NaClO_4$ suspension (A) and in contact with 30 μM $Eu^{III}$ solution (B) after 48 hours of incubation, compared with the background electrolyte. Closed symbols correspond to the forward titration data and open symbols correspond to back titration.

Figure S2. Time dependence in the $Eu^{III}$ removal capacity of *S. bentonitica* cells under aerobic (A and B) and anaerobic (C and D) conditions. The $Eu^{III}$ removal is expressed as mg of Eu per g of dry biomass (A and B) and percentage (B and D).

596 Figure S3. Total organic carbon as a function of time of supernatants obtained after
597 $Eu^{III}$-*S. bentonitica* interaction under anaerobic conditions.

598 Figure S4. Luminescence emission spectra of 30 µM $Eu^{III}$ measured for the supernatants
599 after separating the *S. bentonitica* cells (0.2 g/L) and the re-suspended cells under
600 aerobic conditions at pH 6 and 24 h incubation in 1 M $NaClO_4$ (A). Spectroscopic
601 properties obtained from the $Eu^{III}$-*S. bentonitica* system (B).

602 Table S1. Comparison of deprotonation constants and surface site concentrations for *S.*
603 *bentonitica* and other strains from different studies.

604 Table S2. Main infrared absorption bands of the bacterial cell functional groups

605 Table S3. Luminescence emission data of the $Cm^{III}$-*S. bentonitica* system including
606 those of relevant model systems for comparison.

607

608 **8. Table of content (TOC)/Abstract art**

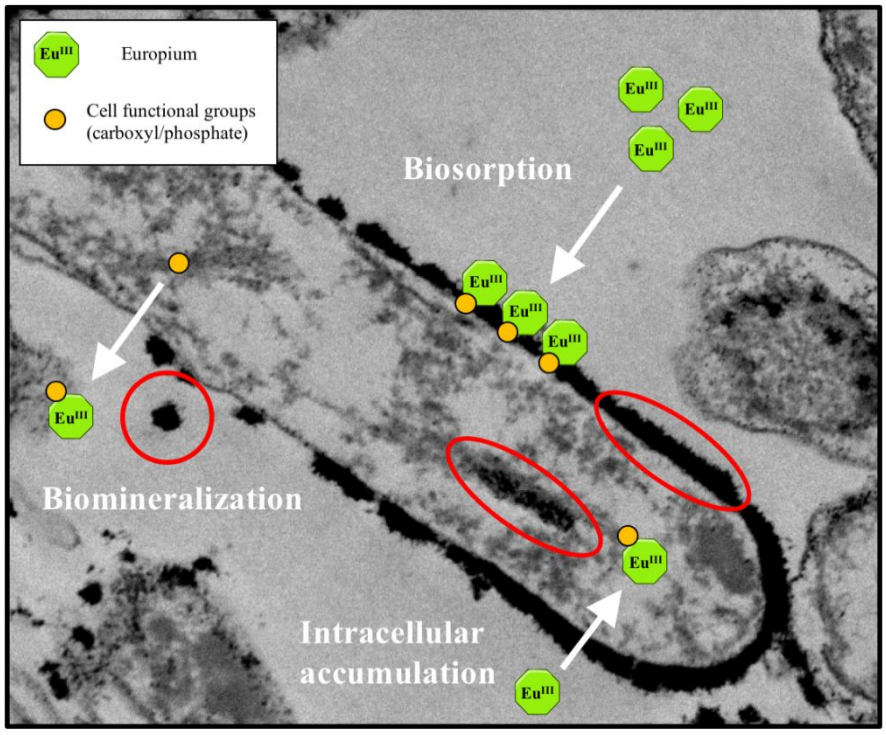


609

## 9. References


(1) NEA. Radioactive Waste in Perspective. Paris, Nuclear Energy Agency. **2010**. https://doi.org/10.1787/9789264092624-en.

(2) Stroes-Gascoyne, S.; Hamon, C. J.; Dixon, D. A.; Martino, J. B. Microbial Analysis of Samples from the Tunnel Sealing Experiment at AECL's Underground Research Laboratory. *Phys. Chem. Earth* **2007**, *32* (1–7), 219–231. https://doi.org/10.1016/j.pce.2006.01.002.

(3) Lopez-Fernandez, M.; Cherkouk, A.; Vilchez-Vargas, R.; Jauregui, R.; Pieper, D.; Boon, N.; Sanchez-Castro, I.; Merroun, M. L. Bacterial Diversity in Bentonites, Engineered Barrier for Deep Geological Disposal of Radioactive Wastes. *Microb. Ecol.* **2015**, *70* (4), 922–935. https://doi.org/10.1007/s00248-015-0630-7.

(4) López-Fernández, M.; Fernández-Sanfrancisco, O.; Moreno-García, A.; Martín-Sánchez, I.; Sánchez-Castro, I.; Merroun, M. L. Microbial Communities in Bentonite Formations and Their Interactions with Uranium. *Appl. Geochemistry* **2014**, *49*, 77–86. https://doi.org/10.1016/j.apgeochem.2014.06.022.

(5) Meleshyn, A. Microbial Processes Relevant for Long-Term Performance of Radioactive Waste Repositories in Clays. Gesellschaft für Anlagen-und Reaktorsicherheit (GRS) mbH. GRS – 291. **2011**. Available from: https://www.grs.de/sites/default/files/pdf/GRS-291.pdf.

(6) Newsome, L.; Morris, K.; Lloyd, J. R. The Biogeochemistry and Bioremediation of Uranium and Other Priority Radionuclides. *Chem. Geol.* **2014**, *363*, 164-184. https://doi.org/10.1016/j.chemgeo.2013.10.034.

(7) Gorietti, D.; Giardina, I.; Arginelli, D.; Battisti, P. Determination of Plutonium, Americium and Curium Isotopes in Radioactive Metal Wastes Deriving from Nuclear Decommissioning. *J. Radioanal. Nucl. Chem.* **2017**, *314* (3), 1785–1792. https://doi.org/10.1007/s10967-017-5553-y.

(8) Kooyman, T.; Buiron, L.; Rimpault, G. A Comparison of Curium, Neptunium and Americium Transmutation Feasibility. *Ann. Nucl. Energy* **2018**, *112*, 748–758. https://doi.org/10.1016/j.anucene.2017.09.041.

(9) Edelstein, N. M.; Klenze, R.; Fanghänel, T.; Hubert, S. Optical Properties of Cm(III) in Crystals and Solutions and Their Application to Cm(III) Speciation. *Coord. Chem. Rev.* **2006**, *250* (7–8), 948–973. https://doi.org/10.1016/J.CCR.2006.02.004.

(10) Ansoborlo, E.; Bion, L.; Doizi, D.; Moulin, C.; Lourenco, V.; Madic, C.; Cote, G.; Van der Lee, J.; Moulin, V. Current and Future Radionuclide Speciation Studies in Biological Media. *Radiat. Prot. Dosimetry* **2007**, *127* (1–4), 97–102. https://doi.org/10.1093/rpd/ncm258.

(11) Shukla, A.; Parmar, P.; Saraf, M. Radiation, Radionuclides and Bacteria: An in-Perspective Review. *J. Environ. Radioact.* **2017**, *180* (11), 27–35. https://doi.org/10.1016/j.jenvrad.2017.09.013.

(12) Moll, H.; Lütke, L.; Bachvarova, V.; Cherkouk, A.; Selenska-Pobell, S.; Bernhard, G. Interactions of the Mont Terri Opalinus Clay Isolate *Sporomusa* sp. MT-2.99 with Curium(III) and Europium(III). *Geomicrobiol. J.* **2014**, *31* (8), 682–696. https://doi.org/10.1080/01490451.2014.889975.

(13) Reitz, T.; Rossberg, A.; Barkleit, A.; Steudtner, R.; Selenska-Pobell, S.; Merroun, M. L. Spectroscopic Study on Uranyl Carboxylate Complexes Formed at the Surface Layer of *Sulfolobus acidocaldarius*. *Dalt. Trans.* **2015,** *44* (6), 2684-2692. https://doi.org/10.1039/c4dt02555e.

(14) Moll, H.; Lütke, L.; Barkleit, A.; Bernhard, G. Curium(III) Speciation Studies with Cells of a Groundwater Strain of *Pseudomonas fluorescens*. *Geomicrobiol. J.* **2013**, *30* (4), 337-346. https://doi.org/10.1080/01490451.2012.688927.

(15) Lopez-Fernandez, M.; Moll, H.; Merroun, M. L. Reversible pH-Dependent Curium(III) Biosorption by the Bentonite Yeast Isolate *Rhodotorula mucilaginosa* BII-R8. *J. Hazard. Mater.* **2018**, *370*, 156-163. https://doi.org/https://doi.org/10.1016/j.jhazmat.2018.06.054.

(16) Bader, M.; Moll, H.; Steudtner, R.; Lösch, H.; Drobot, B.; Stumpf, T.; Cherkouk, A. Association of Eu(III) and Cm(III) onto an Extremely Halophilic Archaeon. *Environ. Sci. Pollut. Res.* **2019**, *26* (9), 9352–9364. https://doi.org/10.1007/s11356-019-04165-7.

(17) Ojeda, J. J.; Romero-González, M. E.; Bachmann, R. T.; Edyvean, R. G. J.; Banwart, S. A. Characterization of the Cell Surface and Cell Wall Chemistry of Drinking Water Bacteria by Combining XPS, FTIR Spectroscopy, Modeling, and Potentiometric Titrations. *Langmuir* **2008**, *24* (8), 4032–4040.

https://doi.org/10.1021/la702284b.

(18) Fein, J. B.; Boily, J. F.; Yee, N.; Gorman-Lewis, D.; Turner, B. F. Potentiometric Titrations of Bacillus Subtilis Cells to Low PH and a Comparison of Modeling Approaches. *Geochim. Cosmochim. Acta* **2005**, *69* (5), 1123–1132. https://doi.org/10.1016/j.gca.2004.07.033.

(19) Krawczyk-Bärsch, E.; Gerber, U.; Müller, K.; Moll, H.; Rossberg, A.; Steudtner, R.; Merroun, M. L. Multidisciplinary Characterization of U(VI) Sequestration by *Acidovorax facilis* for Bioremediation Purposes. *J. Hazard. Mater.* **2018**, *347*, 233–241. https://doi.org/10.1016/j.jhazmat.2017.12.030.

(20) Villar, M. V.; Pérez del Villar, L.; Martín, P. L.; Pelayo, M.; Fernández, A. M.; Garralón, A.; Cuevas, J.; Leguey, S.; Caballero, E.; Huertas, F. J.; Jiméne de Cisneros, C.; Linares, J.; Reyes, E.; Delgado, A.; Fernández-Soler, J. M.; Astudillo, J. The Study of Spanish Clays for Their Use as Sealing Materials in Nuclear Waste Repositories: 20 Years of Progress. *J. Iber. Geol.* **2006**, *32* (1), 15–36.

(21) Ruiz Fresneda, M. A.; Delgado Martín, J.; Gómez Bolívar, J.; Fernández Cantos, M. V.; Bosch-Estévez, G.; Martínez Moreno, M. F.; Merroun, M. L. Green Synthesis and Biotransformation of Amorphous Se Nanospheres to Trigonal 1D Se Nanostructures: Impact on Se Mobility within the Concept of Radioactive Waste Disposal. *Environ. Sci. Nano* **2018**, *5* (9), 2103–2116. https://doi.org/10.1039/c8en00221e.

(22) Sánchez-Castro, I.; Ruiz-Fresneda, M. A.; Bakkali, M.; Kämpfer, P.; Glaeser, S. P.; Busse, H. J.; López-Fernández, M.; Martínez-Rodríguez, P.; Merroun, M. L. *Stenotrophomonas bentonitica* sp. nov., Isolated from Bentonite Formations. *Int. J. Syst. Evol. Microbiol.* **2017**, *67* (8), 2779–2786. https://doi.org/10.1099/ijsem.0.002016.

(23) Omoike, A.; Chorover, J. Spectroscopic Study of Extracellular Polymeric Substances from *Bacillus subtilis*: Aqueous Chemistry and Adsorption Effects. *Biomacromolecules* **2004**, *5* (4), 1219-1230. https://doi.org/10.1021/bm034461z.

(24) Fairley, N. CasaXPS 2.3.17 ed.; Casa Software Ltd. **2006**. Available from: www.casaxps.com

(25) Fein, J. B.; Daughney, C. J.; Yee, N.; Davis, T. A. A Chemical Equilibrium Model for Metal Adsorption onto Bacterial Surfaces. *Geochim. Cosmochim. Acta* **1997**, *61* (16), 3319-3328. https://doi.org/10.1016/S0016-7037(97)00166-X.

(26) Turner, B. F.; Fein, J. B. Protofit: A Program for Determining Surface Protonation Constants from Titration Data. *Comput. Geosci.* **2006**, *32* (9), 1344–1356. https://doi.org/10.1016/j.cageo.2005.12.005.

(27) Borrok, D. M.; Fein, J. B. The Impact of Ionic Strength on the Adsorption of Protons, Pb, Cd, and Sr onto the Surfaces of Gram Negative Bacteria: Testing Non-Electrostatic, Diffuse, and Triple-Layer Models. *J. Colloid Interface Sci.* **2005**. https://doi.org/10.1016/j.jcis.2005.01.015.

(28) Borrok, D.; Turner, B. F.; Fein, J. B. A Universal Surface Complexation Framework for Modeling Proton Binding onto Bacterial Surfaces in Geologic Settings. *Am. J. Sci.* **2005**. https://doi.org/10.2475/ajs.305.6-8.826.

(29) Ngwenya, B. T.; Sutherland, I. W.; Kennedy, L. Comparison of the Acid-Base Behaviour and Metal Adsorption Characteristics of a Gram-Negative Bacterium with Other Strains. *Appl. Geochemistry* **2003**, *18* (4), 527-538. https://doi.org/10.1016/S0883-2927(02)00118-X.

(30) Dittrich, M.; Sibler, S. Cell Surface Groups of Two Picocyanobacteria Strains Studied by Zeta Potential Investigations, Potentiometric Titration, and Infrared Spectroscopy. *J. Colloid Interface Sci.* **2005**, *286* (2), 487-495. https://doi.org/10.1016/j.jcis.2005.01.029.

(31) Yee, N.; Benning, L. G.; Phoenix, V. R.; Ferris, F. G. Characterization of Metal-Cyanobacteria Sorption Reactions: A Combined Macroscopic and Infrared Spectroscopic Investigation. *Environ. Sci. Technol.* **2004**, *38* (3), 775-782. https://doi.org/10.1021/es0346680.

(32) Yee, N.; Fein, J. Cd Adsorption onto Bacterial Surfaces: A Universal Adsorption Edge? *Geochim. Cosmochim. Acta* **2001**, *65* (13), 2037-2042. https://doi.org/10.1016/S0016-7037(01)00587-7.

(33) Claessens, J.; van Lith, Y.; Laverman, A. M.; Van Cappellen, P. Acid-Base Activity of Live Bacteria: Implications for Quantifying Cell Wall Charge. *Geochim. Cosmochim. Acta* **2006**, *70* (2), 267-276. https://doi.org/10.1016/j.gca.2005.09.006.

(34) Merroun, M. L.; Nedelkova, M.; Ojeda, J. J.; Reitz, T.; Fernández, M. L.; Arias, J. M.; Romero-González, M.; Selenska-Pobell, S. Bio-Precipitation of Uranium by Two Bacterial Isolates Recovered from Extreme Environments as Estimated by Potentiometric Titration, TEM and X-Ray Absorption Spectroscopic

Analyses. *J. Hazard. Mater.* **2011**, *197*, 1–10. https://doi.org/10.1016/j.jhazmat.2011.09.049.

(35) Fang, L.; Yang, S.; Huang, Q.; Xue, A.; Cai, P. Biosorption Mechanisms of Cu(II) by Extracellular Polymeric Substances from *Bacillus subtilis*. *Chem. Geol.* **2014**, *386*, 143-151. https://doi.org/10.1016/j.chemgeo.2014.08.017.

(36) Liu, Y.; Alessi, D. S.; Owttrim, G. W.; Petrash, D. A.; Mloszewska, A. M.; Lalonde, S. V.; Martinez, R. E.; Zhou, Q.; Konhauser, K. O. Cell Surface Reactivity of *Synechococcus* sp. PCC 7002: Implications for Metal Sorption from Seawater. *Geochim. Cosmochim. Acta* **2015**, *169*, 30-44. https://doi.org/10.1016/j.gca.2015.07.033.

(37) Ozaki, T.; Gillow, J. B.; Kimura, T.; Ohnuki, T.; Yoshida, Z.; Francis, A. J. Sorption Behavior of Europium(III) and Curium(III) on the Cell Surfaces of Microorganisms. In *Radiochimica Acta*; **2004**, *92* (9-11), 741–748. https://doi.org/10.1524/ract.92.9.741.55006.

(38) Yao, T.; Wu, X.; Chen, X.; Xiao, Y.; Zhang, Y.; Zhao, Y.; Li, F. Biosorption of Eu(III) and U(VI) on *Bacillus subtilis*: Macroscopic and Modeling Investigation. *J. Mol. Liq.* **2016**, *219*, 32-38. https://doi.org/10.1016/j.molliq.2016.01.101.

(39) Gadd, G. M. Biosorption: Critical Review of Scientific Rationale, Environmental Importance and Significance for Pollution Treatment. *J. Chem. Technol. Biotechnol*. **2009**, *84* (1), 13-28. https://doi.org/10.1002/jctb.1999.

(40) Jiang, W.; Saxena, A.; Song, B.; Ward, B. B.; Beveridge, T. J.; Myneni, S. C. B. Elucidation of Functional Groups on Gram-Positive and Gram-Negative Bacterial Surfaces Using Infrared Spectroscopy. *Langmuir* **2004**, *20* (26), 11433-11442. https://doi.org/10.1021/la049043+.

(41) Chu, H. A.; Hillier, W.; Debus, R. J. Evidence That the C-Terminus of the D1 Polypeptide of Photosystem II Is Ligated to the Manganese Ion That Undergoes Oxidation during the S1 to S2 Transition: An Isotope-Edited FTIR Study. *Biochemistry* **2004**, *43* (11), 3152-3166. https://doi.org/10.1021/bi035915f.

(42) Nakamoto, K. Infrared and Raman Spectra of Inorganic and Coordination Compounds: Part B: Applications in Coordination, Organometallic, and Bioinorganic Chemistry, Sixth Edit.; **2008**. https://doi.org/10.1002/9780470405888.

(43) Tackett, J. E. FT-IR Characterization of Metal Acetates in Aqueous Solution. *Appl. Spectrosc.* **1989**, *43* (3), 483-489. https://doi.org/10.1366/0003702894202931.

(44) Deacon, G. B.; Phillips, R. J. Relationships between the Carbon-Oxygen Stretching Frequencies of Carboxylato Complexes and the Type of Carboxylate Coordination. *Coord. Chem. Rev.* **1980**, *33* (3), 227-250. https://doi.org/10.1016/S0010-8545(00)80455-5.

(45) Kumar, S.; Prakash, R.; Singh, V. Synthesis, Characterization, and Applications of Europium Oxide: A Review. *Rev. Adv. Sci. Eng.* **2015**, *4* (4), 247–257. https://doi.org/10.1166/rase.2015.1102.

(46) Pradier, C. M.; Rubio, C.; Poleunis, C.; Bertrand, P.; Marcus, P.; Compère, C. Surface Characterization of Three Marine Bacterial Strains by Fourier Transform IR, X-Ray Photoelectron Spectroscopy, and Time-of-Flight Secondary-Ion Mass Spectrometry, Correlation with Adhesion on Stainless Steel Surfaces. *J. Phys. Chem. B.* **2005**, *109* (19), 9540-9549. https://doi.org/10.1021/jp044705p.

(47) Van Der Mei, H. C.; De Vries, J.; Busscher, H. J. X-Ray Photoelectron Spectroscopy for the Study of Microbial Cell Surfaces. *Surf. Sci. Rep.* **2000**, *39* (1), 1-24. https://doi.org/10.1016/S0167-5729(00)00003-0.

(48) Dufrêne, Y. F.; Van der Wal, A.; Norde, W.; Rouxhet, P. G. X-Ray Photoelectron Spectroscopy Analysis of Whole Cells and Isolated Cell Walls of Gram-Positive Bacteria: Comparison with Biochemical Analysis. *J. Bacteriol.* **1997**, *179* (4), 1023–1028. https://doi.org/10.1128/jb.179.4.1023-1028.1997.

(49) Dufrêne, Y. F.; Rouxhet, P. G. X-Ray Photoelectron Spectroscopy Analysis of the Surface Composition of *Azospirillum brasilense* in Relation to Growth Conditions. *Colloids Surfaces B Biointerfaces* **1996**, *7* (5-6), 271-279. https://doi.org/10.1016/0927-7765(96)01295-7.

(50) Mercier, F.; Alliot, C.; Bion, L.; Thromat, N.; Toulhoat, P. XPS Study of Eu(III) Coordination Compounds: Core Levels Binding Energies in Solid Mixed-Oxo-Compounds EumXxOy. *J. Electron Spectros. Relat. Phenomena.* **2006**, *150* (1), 21-26. https://doi.org/10.1016/j.elspec.2005.08.003.

(51) Merroun, M. L.; Raff, J.; Rossberg, A.; Hennig, C.; Reich, T.; Selenska-Pobell, S. Complexation of Uranium by Cells and S-Layer Sheets of *Bacillus sphaericus* JG-A12. *Appl. Environ. Microbiol.* **2005**, *71* (9), 5532–5543. https://doi.org/10.1128/AEM.71.9.5532-5543.2005.

(52) Fahmy, K.; Merroun, M.; Pollmann, K.; Raff, J.; Savchuk, O.; Hennig, C.; Selenska-Pobell, S. Secondary Structure and Pd(II) Coordination in S-Layer Proteins from *Bacillus sphaericus* Studied by Infrared and X-Ray Absorption Spectroscopy. *Biophys. J.* **2006**, *91* (3), 996-1007. https://doi.org/10.1529/biophysj.105.079137.

(53) Texier, A. C.; Andrés, Y.; Illemassene, M.; Le Cloirec, P. Characterization of Lanthanide Ions Binding Sites in the Cell Wall of *Pseudomonas aeruginosa*. *Environ. Sci. Technol.* **2000**, *34* (4), 610–615. https://doi.org/10.1021/es990668h.

(54) Markai, S.; Andrès, Y.; Montavon, G.; Grambow, B. Study of the Interaction between Europium (III) and *Bacillus subtilis*: Fixation Sites, Biosorption Modeling and Reversibility. *J. Colloid Interface Sci.* **2003**, *262* (2), 351–361. https://doi.org/10.1016/S0021-9797(03)00096-1.

(55) Toyofuku, M.; Nomura, N.; Eberl, L. Types and Origins of Bacterial Membrane Vesicles. *Nat. Rev. Microbiol*. **2019**, *17*, 13-24. https://doi.org/10.1038/s41579-018-0112-2.

(56) Jan, A. T. Outer Membrane Vesicles (OMVs) of Gram-Negative Bacteria: A Perspective Update. *Front. Microbiol.* **2017**, *8*, 1053. https://doi.org/10.3389/fmicb.2017.01053.

(57) Klimentová, J.; Stulík, J. Methods of Isolation and Purification of Outer Membrane Vesicles from Gram-Negative Bacteria. *Microbiol. Res*. **2015**, *170*, 1-9. https://doi.org/10.1016/j.micres.2014.09.006.

(58) Gadd, G. M. Microbial Influence on Metal Mobility and Application for Bioremediation. In *Geoderma*; **2004**, *122* (2-4), 109-119. https://doi.org/10.1016/j.geoderma.2004.01.002.

(59) Niba, E. T. E.; Naka, Y.; Nagase, M.; Mori, H.; Kitakawa, M. A Genome-Wide Approach to Identify the Genes Involved in Biofilm Formation in *E. coli*. *DNA Res.* **2007**, *14* (6), 237–246. https://doi.org/10.1093/dnares/dsm024.

(60) Prigent-Combaret, C.; Vidal, O.; Dorel, C.; Lejeune, P. Abiotic Surface Sensing and Biofilm-Dependent Regulation of Gene Expression in Escherichia Coli. *J. Bacteriol.* **1999**, *181* (19), 5993-6002.

(61) Sánchez-Castro, I.; Bakkali, M.; Merroun, M. L. Draft Genome Sequence of *Stenotrophomonas bentonitica* BII-R7, a Selenite-Reducing Bacterium Isolated from Spanish Bentonites. *Genome Announc.* **2017**, *5* (31). https://doi.org/10.1128/genomeA.00719-17.

(62) Clark, M. E.; Edelmann, R. E.; Duley, M. L.; Wall, J. D.; Fields, M. W. Biofilm Formation in *Desulfovibrio vulgaris* Hildenborough Is Dependent upon Protein Filaments. *Environ. Microbiol.* **2007**, *9* (11). https://doi.org/10.1111/j.1462-2920.2007.01398.x.

(63) Rui, X.; Kwon, M. J.; O'Loughlin, E. J.; Dunham-Cheatham, S.; Fein, J. B.; Bunker, B.; Kemner, K. M.; Boyanov, M. I. Bioreduction of Hydrogen Uranyl Phosphate: Mechanisms and U(IV) Products. *Environ. Sci. Technol.* **2013**, *47* (11), 5668–5678. https://doi.org/10.1021/es305258p.